Digitising sandbox experiments using open-source Structure-from-Motion/photogrammetry/Digital Image Correlation package MicMac

Olivier Galland[1], Luc Girod[2], Sonja H. M. Greiner[3,4,5], Pauline Souloumiac[6], Frank B. B. Guldstrand[1,7], Håvard S. Bertelsen[2], Daniel Yagupsky[9]

Affiliations

[1] The Njord Centre, Department of Geosciences, University of Oslo, Norway

[2] Department of Geosciences, University of Oslo, Norway

[3] Nordic Volcanological Center, Institute of Earth Sciences, University of Iceland, Reykjavík, Iceland

[4] Department of Earth Sciences, Uppsala University, Uppsala, Sweden

[5] Center for Natural Hazard and Disaster Science (CNDS), Sweden

[6] Laboratoire Géosciences et Environnement Cergy, CY Cergy Paris Université, France

[7] Swedish Defence Research Agency, Sweden

[8] CONICET-IDEAN, Instituto de Estudios Andinos "Don Pablo Groeber", Universidad de Buenos Aires, Buenos Aires, Argentina

This paper is a non-peer reviewed preprint submitted to EarthArXiv. It has been submitted for peer review as a book chapter in upcoming book entitled "Virtual Geoscience: Capturing and Working with the Earth in 3D", to be published by the Geological Society.

1 Introduction

Digitisation of outcrops has been revolutionary for modern and quantitative geosciences. Modern tools such as LIDAR scanning and Structure-from-Motion/photogrammetry allow producing virtual models of outcrops that can be analysed subsequently on the computer (Buckley *et al.* 2010a), saving weeks of fieldwork time. Even though outcrop digitisation will never replace on-site field work, these techniques allow (1) detailed mapping of otherwise inaccessible outcrops, i.e. cliffs (Galland *et al.* 2019), (2) quantitative measurements of e.g. fractures and lateral lithological variations of large outcrops (Buckley *et al.* 2010b; Buckley *et al.* 2019; Sleveland *et al.* 2020), (3) revisiting the outcrop over and over again, (4) capture geophysical-scale outcrops (Eide *et al.* 2017; Rabbel *et al.* 2018), and (6) sharing outcrops for educational purposes via virtual field trips (Senger *et al.* 2021; Pugsley *et al.* 2022).

Laboratory modelling in geosciences similarly experienced a quantitative digital revolution (Leever *et al.* 2014). Both LIDAR and SfM/Photogrammerty were also implemented to quantify deformation of sandbox models, as well as Digital Image Correlation (DIC)(Delcamp *et al.* 2008; Leever *et al.* 2011; Abdelmalak *et al.* 2012; Farzipour-Saein *et al.* 2013; Visage *et al.* 2023). While laboratory modelling has been overlooked for a long time in the geoscience community with respect to numerical modelling, these new quantitative tools brought laboratory modelling to a new dimension (Kervyn *et al.* 2010; Adam *et al.* 2013; Poppe *et al.* 2019). The resulting quantitative data became essential for making sandbox models proper physics experiments.

Structure-from-Motion and photogrammetry have been implemented in sandbox models to monitor deformation of their surface (Donnadieu *et al.* 2003; Schmiedel *et al.* 2019; Bertelsen *et al.* 2021; Rincón *et al.* 2022). Various software packages are available, either open-source of commercial. Some commercial packages are intuitive press-button equipment (Michail *et al.* 2021); these can be very practical to use, but they can be very expensive and unaffordable for most academic laboratories. Another option is open-source alternatives, such as MicMac (Rupnik *et al.* 2017). MicMac is a versatile open-source package that includes, among others, Structure-from-Motion, photogrammetry and Digital Image Correlation. It has been for various purposes, including geosciences (Rosu *et al.* 2015; Girod *et al.* 2017), architecture (Murtiyoso and Grussenmeyer 2017; Rupnik *et al.* 2017) and biophysics (Combriat *et al.* 2024). MicMac has been successfully applied to monitor surface deformation in sandbox models (Galland *et al.* 2016; Schmiedel *et al.* 2017; Schmiedel *et al.* 2019; Bertelsen *et al.* 2021; Visage *et al.* 2023). However, the use of MicMac is not user-friendly, and the steep learning curve of how to use it, and even to install it, can make it repellent for geoscientists that are less familiar with computers and command-line based programs.

To overcome this, we provide in this paper a detailed workflow to install and use MicMac as a very effective tool to monitor and digitise surfaces of deforming sandbox models. We will describe how to (1) calibrate synchronized cameras and improve model surfaces for optimal results, (2) install and run MicMac in various OS, and (3) load and plot maps of the digital data (topography, displacements, divergence, shear strain) using Matlab scripts.

2 Laboratory setup

2.1 Preparing the apparatus

Good results from photogrammetry start with good laboratory procedure to acquire the best possible images (Figure 1). This section describes the different steps of the sandbox model preparation to ensure that photogrammetry calculations provide good results. Table 1 lists the main steps of to implement for the preparation of the model surface and of the monitoring system.

2.2 Camera triggering system

There are potentially as many triggering systems as there are types of cameras, therefore we do not describe here a method for triggering the cameras. What is important to have in mind is that the cameras need to be triggered at the same time, or the time difference between the shots need to be considerably shorter than the time scale of the models. If for example the time scale of a model is several hours, it is acceptable to have a couple of second time lag between the shots of the distinct cameras. In this case, it is possible to trigger the cameras manually one camera after the others with a remote, or to use the internal intervalometer of the cameras.

However, we recommend building a system that automatically triggers all the cameras synchronously, or to use open-source camera-controlling software such as digiCamControl (https://digicamcontrol.com/). In the laboratory of the University of Oslo, we designed triggering systems based on the open-source Arduino electronic system. The detailed construction of the electronics and Arduino codes are provided in Håvard Bertelsen's PhD thesis (https://archive.sigma2.no/pages/public/datasetDetail.jsf?id=10.11582/2024.00066, folder 1_Literature).

2.3 Calibration of the camera system

It is crucial to prepare and calibrate the cameras to ensure as good and precise results as possible. This step is not necessary if all cameras are different models. If some of the cameras are of the same model, apply the procedure described in Table 2 for these cameras. The reason is that MicMac reads the name of the camera model contained in the exif data of the images: if MicMac reads the same camera model and the same focal length, MicMac will treat the images as if they were shot with the same camera having the same distortion model, which would be incorrect. For the calibration, we invite the modeller to use a similar target as that used for the GCPs (see Figure 1C).

3 Installing MicMac

3.1 Computer specifications

While Micmac is designed to run on even modest hardware, processing speed scales directly with the computer's performance. MicMac is particularly reliant on a strong CPU and makes use of all the cores available in several of the processing steps. It is, however, rather light in its use of RAM, typically using less than 400MB/core. It also profits immensely from fast storage solutions, such as PCIe SSDs, and remote storage is to be avoided. At the time of writing, MicMac does not take advantage of GPU (graphics card).

Note that MicMac can be installed on both Linux, Windows and MacOS (Table 3). However, the semi-automated scripts that call MicMac functions described in this contribution are bash scripts (see section "Running MicMac") executable only on Linux and MacOS, but not on Windows. To be used on Windows, these Bash scripts would need to be converted to Windows-compatible Batch scripts. We decided to provide only the Bash scripts version, not their Windows-compatible Batch equivalent. To use these Bash scripts on Windows, we describe in Table 3 how modellers need to install Windows Subsystem for Linux, which is a form of virtual machine running Ubuntu. Thus, the modeller can run Linux on her/his Windows computer, and use the Bash scripts we provide.

3.2 Installation procedures

Micmac's source code and binary releases are available on the project's GitHub page: https://github.com/micmacIGN/micmac, where the latest release can be found on the right side of the page. Clicking on "Latest" brings the user to a new page where a Linux version (MicMac_Linux.tgz) can be found, as well as the source code.

Note that MicMac is for the most part a command line tool, and not a GUI (Graphical User Interface) based software, to the exception of masking and ground control point input tools. We describe in Table 3 and in Appendix A and B how to install MicMac on different OS (https://archive.sigma2.no/pages/public/datasetDetail.jsf?id=10.11582/2024.00066, folder 4_Appendix).

4 The workflows

The main functions of the photogrammetric workflow using MicMac are listed in Table 4 and their order is displayed in Figure 2. The online documentation of the MicMac functions is available on the following Github repository: https://github.com/micmacIGN/Documentation/). Ready-to-use workflows are available on the Sigma2 Norwegian data archive system (https://archive.sigma2.no/pages/public/datasetDetail.jsf?id=10.11582/2024.00066, folder 2_Workflows). There are four workflows available:

- *test_to_improve_SfM* - This workflow is to be used to test the model preparation procedure to optimise the result quality of the Structure-from-Motion/Photogrammetry results (see section "Improving data quality from existing tests").

- *topo* - This workflow is designed only to compute time sequence of topographic maps.

- *topo_inc_horiz_displ* - This workflow is designed to compute time sequence of both topographic maps and incremental horizontal displacements. This workflow applies if horizontal displacements in the models are large, i.e. larger than the maximum displacement detectable by the digital image correlation function (see section "Structure-from-Motion").

- *topo_tot_horiz_displ* - This workflow is designed to compute time sequence of both topographic maps and total horizontal displacements. This workflow applies if total horizontal displacements in the models are smaller than the maximum displacement detectable by the digital image correlation function (see section "Structure-from-Motion").

After selecting the relevant workflow, the user copies all the files of the corresponding folder and pastes them in a folder of the experiment to process (Experiment_Folder of Figure 3). The following sections apply to the four workflows.

5 Preparing the data

The scripts shared with this contribution are designed to work in a specific folder structure of the data. Below we describe how to prepare the data before running MicMac. Instructions for preparing the data are also available on a YouTube tutorial (https://youtu.be/f5-UUaFy61g).

- In the folder of the experiment (Experiment_Folder), create as many folders as the number of cameras. Name the folders *Camera1*, *Camera2*, etc. (Figure 3, left).
- Copy the images of the Camera1 in folder *Camera1*, images of Camera2 in folder *Camera2*, etc. Make sure that each folder contains the same number of images.
- In the folder of the experiment, make sure the files `01_rename_and_sort.sh`, `02_ground_control_points.sh`, and `03_workflow_full.sh` are copied in, as well as files *GCPs.txt* and *MicMac-LocalChantierDescripteur.xml*.
- Open first the shell script `01_rename_and_sort.sh`. This code will create a new folder *input*, in which it will create folders corresponding to the time steps of the monitoring. These folders are named *000*, *001*, etc. Folder *000* corresponds to the initial surface of the model. Then the code will copy the first image of each camera folder in folder *input/000*, and rename them *1.JPG*, *2.JPG*, etc. (Figure 3). It will implement the same procedure for all other time steps.

- The structure of `01_rename_and_sort.sh` consists of several blocks of lines that correspond to a given camera. The blocks have the same structure, except the first one which has one additional line. By default, this code is designed for three cameras (Figure 4). To add a camera, copy the lines corresponding to one camera and replace camera folder name and the camera name by the correct ones (Figure 4). To remove a camera, delete the corresponding lines of code. Never delete the lines for Camera1 (Figure 4).
- Run code `01_rename_and_sort.sh` in a Terminal window. To do this, in the Terminal go in the experiment folder by typing `cd /path/to/experiment_folder/`. Make sure code `01_rename_and_sort.sh` is executable, and run it by typing in the Terminal `./01_rename_and_sort.sh`.

Once this code is run, the data is now ready to be processed with MicMac.

6 Running MicMac

Running functions of MicMac is done through codes `02_ground_control_points.sh`, and `03_workflow_full.sh`. The instructions described in the following sections are also described in great details on a YouTube tutorial (https://youtu.be/f5-UUaFy61g).

6.1 Georeferencing the models

Because modellers aim to produce quantitative data, the models needs to be properly oriented and at correct scale, which requires georeferencing. The georeferencing necessitates to define Ground Control Points (GCPs). The X, Y and Z coordinates of the GCPs are to be measured precisely in a coordinate system defined by the modeller. Note that the units of the GCP coordinates are in meter. The georeferencing process is done through running shell script

02_ground_control_points.sh in a Terminal window. The detailed use of this script is described in Appendix C (https://archive.sigma2.no/pages/public/datasetDetail.jsf?id=10.11582/2024.00066, in folder 4_Appendix).

6.2 Definition of camera specifications

An important parameter to ensure relevance of the calculation is the specifications of the cameras used for the monitoring, especially the sensor size. This subsection describes the method to define the cameras and their sensor size.

The camera definition is done through file MicMac-LocalChantierDescripteur.xml (see location in Figure 3). Figure 5 displays a characteristic example of the structure of file MicMac-LocalChantierDescripteur.xml. The file consists of two parts: a first part used to define the used camera models and their specifications, a second part used to associate the camera models with the processed images. In the example of Figure 5, four cameras were used with two distinct camera models (Nikon D3300 and Canon EOS 80D).

In the first section, one needs to define the names of the camera models and their sensor size (always write small number first)(Figure 5). In the second section, the user defines the camera model that has been used to shoot each photograph. The names of the photographs should be the same as those produced from script 01_rename_and_sort.sh, in agreement with the right location of the cameras (Figure 1).

Note that in the example given in Figure 5, the same camera (Nikon D3300) is used for photographs 1.JPG, 2.JPG and 3.JPG, whereas in reality, these photographs were shot using distinct Nikon D3300 cameras. This procedure is valid if the three cameras have been calibrated following the instructions of section "Calibration of the camera system". If such a calibration cannot be implemented, the user needs to define three distinct cameras with (1) the same sensor size and (2) three distinct names, e.g. NikonD3300_1, NikonD3300_2 and NikonD3300_3. Note, however, that this later procedure implies more camera parameters to be found by MicMac, resulting in a less stable Structure-from-Motion calculations with higher potential of failure.

6.3 Structure-from-Motion

The structure-from-Motion is implemented in shell script `03_workflow_full.sh`. Running this script calculates automatically the required data for all time steps of an experiment. We provide several versions of this script, which implement distinct workflows depending on the purpose of the monitoring: (1) computing of topography (DEM and ΔDEM), (2) computing of topography and total horizontal displacements if displacements are small (DEM and ΔDEM, U_X and U_Y), and (3) computing of topography and incremental horizontal displacements if displacements are small (DEM and ΔDEM, U_X and U_Y).

All versions of script `03_workflow_full.sh` share the same variables, that can be manually modified by changing their values in the first lines of the script (Figure 6). The variables to modify are the following: `BOX='[x_min,y_min,x_max,y_max]'`, `INIT`, `NrofIm`, `Uncertainty`, `SizeCorrWind`. Note that both variables `Uncertainty` and `SizeCorrWind` are only relevant for workflows calculating horizontal displacements. Table 5 lists these parameters and their meaning.

6.4 Outputs

The outputs of the calculations after running `03_workflow_full.sh` are contained in the newly created folder *output*, in which folders *000*, *001*, etc., are also created (Figure 3). Table 6 describes in detail the output files produced by `03_workflow_full.sh`. Note that

`03_workflow_full.sh` script also produces .ply files, which are point clouds displayed in 3D. They can be opened using open-source software Meshlab or CloudCompare. File CAM_Abs.ply displays (1) the tie points computed from functions Tapioca and Tapas (Figure 2) and (2) the computed positions of the cameras (Figure 7).

7 Loading and plotting the data

In addition to the scripts that implement MicMac, we also provide Matlab codes to plot the topographic and displacement data. These codes produce the following:

- Topographic maps (*DEM*);
- Maps of topography change with respect to initial topography (*U_DEM*);
- Maps of U_x and U_y, i.e. displacements parallel to X-axis and Y-axis, respectively, defined by the georeferencing procedure (see section Georeferencing the models);
- Maps of divergence, shear strain and second invariant of strain tensor. The divergence, shear strain and second invariant maps are calculated from the U_x and U_y maps using the formulas $\mathrm{div}(\vec{U}) = \partial U_x/\partial x + \partial U_y/\partial y$, $\gamma_{xy} = 1/2\left(\partial U_x/\partial y + \partial U_y/\partial x\right)$, $I_2 = -\partial U_x/\partial x \cdot \partial U_y/\partial y + \left(1/2\left(\partial U_x/\partial y + \partial U_y/\partial x\right)\right)^2$, respectively.
- Values of maximum and minimum values of *DEM*, *U_DEM*, U_x, U_y, divergence and shear strain to set optimal colour scales;
- Options to plot maps with background image and shaded relief of topography.

Figure 8 displays characteristic examples of data maps produced by the Matlab scripts provided with this contribution.

7.1 Structure of Matlab code package

The code package consists of a series of Matlab codes that are linked together. It should be placed in a folder called "matlab_scripts", that is inside the experiment folder (Figure 3). The codes and their functions are listed and described in Table 7. Note that code `00_Master_code.m` will call `01_input_parameters.m` in the same folder, and the other codes (`02_DEM_load_scale.m`, `03_DEM_plot.m`, `04_Displacement_load_scale.m`, `05_displacement_strain_divergence_plot.m`, `06_MovieAndGifAnimator.m`) contained in folder `codes`. Note as well that codes `04_Displacement_load_scale.m`, `05_displacement_strain_divergence_plot.m` will be implemented only in workflows *topo_inc_horiz_displ* and *topo_inc_horiz_displ* (see section "The workflows") because horizontal displacements are not computed in the other workflows.

7.2 List of input parameters

The input variable parameters, and their meaning, in `01_input_parameters.m` are listed in Table 8. This list of parameters allows the modeller to design figures with large flexibility.

8 Improving data quality from existing tests

The quality of the processing depends on (1) the quality of the calibration of the cameras and (2) the quality of the texture at the model surface. It can be challenging for an inexperienced modeller to implement good quality calibration and model surface texture from the first model. Fortunately, the outputs of MicMac provide some data that will help the modeller to quantify the quality of the results produced from MicMac, and so to improve her/his procedure. Appendix D (https://archive.sigma2.no/pages/public/datasetDetail.jsf?id=10.11582/2024.00066, in folder 4_Appendix) describes with great details the procedure that helps the modeller to improve data quality.

9 Examples

This section present characteristic results produced from the workflows described and shared with this contribution. We also share the laboratory data plotted in the figures, so that the modeller can train using our workflows. The data are available on the Sigma2 Norwegian data archive (https://archive.sigma2.no/pages/public/datasetDetail.jsf?id=10.11582/2024.00066, folder 3_Dataset).

9.1 Dyke-induced surface deformation

Magma is commonly transported through the Earth's crust through sheet intrusions. This makes the understanding of sheet intrusions and especially dyke propagation and the associated surface deformation important for hazard assessment and monitoring of volcanically active areas. Analogue models can help to study specific aspects of intrusion processes or the effect of individual parameters such as the physical properties of the host rock or fluid on a laboratory scale and in controlled conditions. We present here an example of laboratory experiments to study magmatic intrusion processes and their associated surface deformation.

The emplacement of a magmatic intrusion was modelled by injecting molten vegetable oil into a brittle plastic Coulomb-material consisting of 90% micro glass beads (90%) and Silica flour (10%). Both the analogue magma and the analogue host rock have been previously used to model sheet intrusions with similar experimental setups and represent the intrusions of magma into host rock of weak to intermediate cohesion (Galland *et al.* 2006; Galland 2012; Galland *et al.* 2014; Schmiedel *et al.* 2019; Bertelsen *et al.* 2021).

The molten oil is injected through the base of a 39 cm x 38 cm box filled with the analogue host rock at a temperature of 50°C and constant flow rate of 20 ml/min, which is controlled by a volumetric pump (Figure 9). Prior to injection, the analogue host rock has been compacted using a compressed air shaker to ensure a uniform, reproducible density. The compacted material has a thickness of 6cm and is covered by a thin layer of ground coffee powder and olivine sand to provide surface texture for feature tracking in post-processing. A synchronized array of four cameras was placed above the injection box and recorded images of the model surface at a 1s-framing rate. Although injected in a liquid state, the vegetable oil solidifies at room temperatures. This allows to excavate the intrusion after the experiment and to observe the final intrusion geometry, which can be translated into a digital 3D model through photogrammetry and SfM using Agisoft Metashape. Observations of the model surface were processed using MicMac and postprocessed in Matlab. Using GCPs in a common reference frame for the intrusion model and the surface deformation data allows to correlate them, which was done using ParaView.

During the early stages of the intrusion process, deformation is characterized by gently sloped, subcircular, low amplitude doming centered around the injection inlet (Figure 10A). Then the uplift becomes more concentrated and shifts towards the left (Figure 10C and E). Eventually, the oil breaches the model surface at the edge of the area with the highest uplift (Figure 10G).

Horizontal deformation gradients are concentrated along discrete lines, which either belong to a network of radial lines experiencing positive divergence, i.e. extension (Figure 10B) or a surrounding ring with a negative divergence, which corresponds to compression/shortening (Figure 10D). The compression falls close to the edge of the uplifting area (Figure 10C and D). As the uplift pattern concentrates on the left, a linear segment of extension is observed which is perpendicular to radial direction of most of the previously observed extensional features (Figure 10F). This extensional feature meets the edge of the initially compressed area simultaneous to the oil breaching the surface (Figure 10H).

The final intrusion shape is a partial cone sheet, which connects the injection inlet with the eventual "eruptive fissure" (Figure 11).

It is well known from observations in nature and laboratories, as well as quantitative models that surface deformation patterns become more concentrated as a propagating intrusion approaches the surface (Okada, 1985; Dzurisin, 2007; Guldstrand et al., 2018). This explains well the shift of the maximum deformation as the inclined intrusion propagates upwards. Both the intrusion shape and associated surface deformation agree well with previous, similar experiments by Schmiedel *et al.* (2019). They suggested that the radial, extensional features correspond to surface cracks during doming and that the compression around the dome corresponds to shear damage zones which form ahead of the intrusion and along which the intrusion propagates to the surface. The tensional feature above the area of maximum uplift has comparable dimensions to the length of the underlying intrusion and was possibly caused by the propagating intrusion tip dilating the shear zone at depth.

By providing detailed information about both the intrusion geometry and the associated surface deformation, quantitative laboratory experiments can provide valuable insights into volcanic processes and aid monitoring of active volcanic systems, where detailed, direct observations of magmatic intrusions are not common and the spatial or temporal resolution of surface deformation may be strongly limited.

9.2 Strike-slip faulting experiment

This section presents a strike-slip fault experiment carried out in the analogue laboratory of the Geosciences and Environment Cergy (GEC) laboratory of CY Cergy Paris University (CYU).

The experimental prototype consists of a sandbox, four cameras located above the box and a motor driving a mobile plate (Figure 12).

The box is made up of two PVC plates of 1500 mm x 670 mm each, one of which is fixed and the other is mobile. There is a pre-existing linear fault at the base of the model (dotted line on the Figure 12). The mobile plate is set in motion by the motor and the fault develops in the middle of the box located at the base of the dotted line. The sandbox side walls are far enough apart to avoid edge effects.

The photos were taken with four cameras located one metre above the model (Nikon 3200 with an 18 mm lens). Three of them are arranged in an equilateral triangle at an angle chosen to capture uplift at the surface. The fourth camera is positioned above the model looking straight downwards. Each picture is taken every 0.5 mm of displacement of the underlying plate; the resolution of the images was 0.18 mm per pixel.

The study area (grey rectangle) presented in the following figures is a mask of dimensions 900 mm x 220 mm. The model is made entirely of Fontainebleau aeolian quartz sand, with a median grain size of 250 µm. The sand pack is manually poured into the box and has a static internal friction of 33.4°, a dynamic friction of 34.2°, and a density of 1680 kg/m^3 with an unknown uncertainty due to the manual mode of deposit (Maillot 2013). The thickness of the sand pack is 6 cm. As sand has very little cohesion, the thickness of the sand corresponds in nature to the depth of the frictional crust. We have therefore chosen an arbitrary length scale: 6 cm in the model corresponds to 6 km in nature (Figure 12). The total displacement applied by the motor is 150 mm.

We calculated the horizontal and vertical displacement at the surface of the model as well as the shear deformation for two stages in the evolution of the fault, presented in the following Figure 13A (9 mm of cumulative displacement) and Figure 13B (18 mm of cumulative displacement). We obtained horizontal displacement and shear deformation by image correlation (9x9 pixel frame). We calculated the vertical displacement by subtracting the digital surface models from two displacement steps.

10 Conclusions

This chapter describes workflows that implement the open-source Structure-from-Motion/Photogrammetry software MicMac for monitoring and digitising surface deformation of analogue models. Though MicMac is not user-friendly, the workflows described in this chapter are designed to be used by modellers who are not familiar with computers and scripting.

The main steps of the workflow description are the following:

- we first explain how the laboratory procedure to prepare the model surface and locate and calibrate cameras to perform the monitoring.
- We describe how to install MicMac on various OS (Microsoft Windows, MacOS, Linux Ubuntu).
- We provide several MicMac workflows: a workflow for helping the modeller to improve the procedure, a workflow to compute time series of topographic maps, and workflow to compute time series of both topographic maps and maps of incremental horizontal displacements (for models with large total displacements, i.e. tectonic models), and finally a workflow to compute time series of both topographic maps and maps of total horizontal displacements (for models with small total displacements).
- We explain how to structure and prepare the data to ensure success of the processing, and how to run the MicMac scripts provided with this chapter.
- With each workflow, we provide a suite of Matlab scripts to plot maps of the computed data, and we describe the input parameters to produce appealing maps.

Finally, we describe two model examples, a model of magma intrusion with small total displacements of the model surface, and a model of strike-slip faulting with large total displacements of the model surface. The data and workflows described and mentioned in this chapter are available on the Sigma2 Norwegian data archive (https://archive.sigma2.no/pages/public/datasetDetail.jsf?id=10.11582/2024.00066).

11 Acknowledgements

The workflows presented in this contribution were designed under the framework of the DIPS project funded by the Research Council of Norway (grant no. 240467), which covered Guldstrand's position. Bertelsen’s position was funded by the Faculty of Mathematics and Natural Sciences of the University of Oslo.

12 References

Abdelmalak, M.M., Mourgues, R., Galland, O. and Bureau, D. 2012. Fracture mode analysis and related surface deformation during dyke intrusion: Results from 2D experimental modelling. *Earth and Planetary Science Letters*, **359-360**, 93-105, https://doi.org/10.1016/j.epsl.2012.10.008.

Adam, J., Klinkmüller, M., Schreurs, G. and Wieneke, B. 2013. Quantitative 3D strain analysis in analogue experiments simulating tectonic deformation: Integration of X-ray computed tomography and digital volume correlation techniques. *Journal of Structural Geology*, **55**, 127-149, https://doi.org/http://dx.doi.org/10.1016/j.jsg.2013.07.011.

Bertelsen, H.S., Guldstrand, F., Sigmundsson, F., Pedersen, R., Mair, K. and Galland, O. 2021. Beyond elasticity: Are Coulomb properties of the Earth's crust important for volcano geodesy? *Journal of Volcanology and Geothermal Research*, **410**, 107153, https://doi.org/https://doi.org/10.1016/j.jvolgeores.2020.107153.

Buckley, S.J., Enge, H.D., Carlsson, C. and Howell, J.A. 2010a. Terrestrial laser scanning for use in virtual outcrop geology. *The Photogrammetric Record*, **25**, 225-239, https://doi.org/10.1111/j.1477-9730.2010.00585.x.

Buckley, S.J., Schwarz, E., Terlaky, V., Howell, J.A. and Arnott, R.W. 2010b. Combining aerial photogrammetry and terrestrial lidar for reservoir analog modeling. *Photogrammetric Engineering & Remote Sensing*, **76**, 653-963.

Buckley, S.J., Ringdal, K., Naumann, N., Dolva, B., Kurz, T.H., Howell, J.A. and Dewez, T.J.B. 2019. LIME: Software for 3-D visualization, interpretation, and communication of virtual geoscience models. *Geosphere*, **15**, 222-235, https://doi.org/10.1130/GES02002.1.

Delcamp, A., van Wyk de Vries, B. and James, M.R. 2008. The influence of edifice slope and substrata on volcano spreading. *Journal of Volcanology and Geothermal Research*, **177**, 925-943, https://doi.org/10.1016/j.jvolgeores.2008.07.014.

Donnadieu, F., Kelfoun, K., van Wyk de Vries, B., Cecchi, E. and Merle, O. 2003. Digital photogrammetry as a tool in analogue modelling: applications to volcano instability. *Journal of Volcanology and Geothermal Research*, **123**, 161-180, https://doi.org/10.1016/s0377-0273(03)00034-9.

Eide, C.H., Schofield, N., Lecomte, I., Buckley, S.J. and Howell, J.A. 2017. Seismic Interpretation of Sill-Complexes in Sedimentary Basins: The 'Sub-Sill Imaging Problem. *Journal of the Geological Society*, **175**, 193-209.

Farzipour-Saein, A., Nilfouroushan, F. and Koyi, H. 2013. The effect of basement step/topography on the geometry of the Zagros fold and thrust belt (SW Iran): an analog modeling approach. *International Journal of Earth Sciences*, **102**, 2117-2135, https://doi.org/10.1007/s00531-013-0921-5.

Galland, O. 2012. Experimental modelling of ground deformation associated with shallow magma intrusions. *Earth and Planetary Science Letters*, **317-318**, 145-156, https://doi.org/10.1016/j.epsl.2011.10.017.

Galland, O., Cobbold, P.R., Hallot, E., de Bremond d'Ars, J. and Delavaud, G. 2006. Use of vegetable oil and silica powder for scale modelling of magmatic intrusion in a deforming brittle crust. *Earth and Planetary Science Letters*, **243**, 786-804.

Galland, O., Burchardt, S., Hallot, E., Mourgues, R. and Bulois, C. 2014. Dynamics of dikes versus cone sheets in volcanic systems. *Journal of Geophysical Research: Solid Earth*, 2014JB011059, https://doi.org/10.1002/2014jb011059.

Galland, O., Bertelsen, H.S. *et al.* 2016. Application of open-source photogrammetric software MicMac for monitoring surface deformation in laboratory models. *Journal of Geophysical Research: Solid Earth*, **121**, 2852—2872, https://doi.org/10.1002/2015JB012564.

Galland, O., Spacapan, J.B. *et al.* 2019. Structure, emplacement mechanism and magma-flow significance of igneous fingers – Implications for sill emplacement in sedimentary basins. *Journal of Structural Geology*, **124**, 120–135, https://doi.org/https://doi.org/10.1016/j.jsg.2019.04.013.

Hebeler, F. 2023. hillshade, https://www.mathworks.com/matlabcentral/fileexchange/14863-hillshade

Kervyn, M., Boone, M.N., van Wyk de Vries, B., Lebas, E., Cnudde, V., Fontijn, K. and Jacobs, P. 2010. 3D imaging of volcano gravitational deformation by computerized X-ray micro-tomography. *Geosphere*, **6**, 482-498, https://doi.org/10.1130/ges00564.1.

Leever, K.A., Galland, O. and Acocella, V. 2014. The Science Behind Laboratory-Scale Models of the Earth. *Eos, Transactions American Geophysical Union*, **95**, 30-30, https://doi.org/10.1002/2014eo030008.

Leever, K.A., Gabrielsen, R.H., Sokoutis, D. and Willingshofer, E. 2011. The effect of convergence angle on the kinematic evolution of strain partitioning in transpressional brittle wedges: Insight from analog modeling and high-resolution digital image analysis. *Tectonics*, **30**, TC2013, https://doi.org/10.1029/2010tc002823.

Lowe, D.G. 2004. Distinctive Image Features from Scale-Invariant Keypoints. *International Journal of Computer Vision*, **60**, 91-110, https://doi.org/10.1023/b:visi.0000029664.99615.94.

Maillot, B. 2013. A sedimentation device to produce uniform sand packs. *Tectonophysics*, **593**, 85-94, https://doi.org/http://dx.doi.org/10.1016/j.tecto.2013.02.028.

Michail, M., Rudolf, M., Rosenau, M., Riva, A., Gianolla, P. and Coltorti, M. 2021. Shape of plutons in crustal shear zones: A tectono-magmatic guide based on analogue models. *Journal of Structural Geology*, **150**, 104417, https://doi.org/https://doi.org/10.1016/j.jsg.2021.104417.

Poppe, S., Holohan, E.P. *et al.* 2019. An inside perspective on magma intrusion: quantifying 3D displacement and strain in laboratory experiments by dynamic X-Ray computed tomography. *Frontiers in Earth Science*, **7**, https://doi.org/10.3389/feart.2019.00062.

Pugsley, J.H., Howell, J.A. *et al.* 2022. Virtual field trips utilizing virtual outcrop: construction, delivery and implications for the future. *Geoscience Communication*.

Rabbel, O., Galland, O., Mair, K., Lecomte, I., Senger, K., Spacapan, J.B. and Manceda, R. 2018. From field analogues to realistic seismic modelling: a case study of an oil-producing andesitic sill complex in the Neuquén Basin, Argentina. *Journal of the Geological Society*, https://doi.org/10.1144/jgs2017-116.

Reeves, G. 2023. smooth2a, https://www.mathworks.com/matlabcentral/fileexchange/23287-smooth2a

Rincón, M., Márquez, A., Herrera, R., Galland, O., Sánchez-Oro, J., Concha, D. and Montemayor, A.S. 2022. Monitoring Volcanic and Tectonic Sandbox Analogue Models Using the Kinect v2 Sensor. *Earth and Space Science*, **9**, e2020EA001368, https://doi.org/https://doi.org/10.1029/2020EA001368.

Rosu, A.-M., Pierrot-Deseilligny, M., Delorme, A., Binet, R. and Klinger, Y. 2015. Measurement of ground displacement from optical satellite image correlation using the free open-source software MicMac. *ISPRS Journal of Photogrammetry and Remote Sensing*, **100**, 48-59, https://doi.org/http://dx.doi.org/10.1016/j.isprsjprs.2014.03.002.

Rupnik, E., Daakir, M. and Pierrot Deseilligny, M. 2017. MicMac – a free, open-source solution for photogrammetry. *Open Geospatial Data, Software and Standards*, **2**, 14, https://doi.org/10.1186/s40965-017-0027-2.

Schmiedel, T., Galland, O. and Breitkreuz, C. 2017. Dynamics of sill and laccolith emplacement in the brittle crust: role of host rock strength and deformation mode. *Journal of Geophysical Research: Solid Earth*, **122**, 8625-9484, https://doi.org/10.1002/2017JB014468.

Schmiedel, T., Galland, O., Haug, Ø.T., Dumazer, G. and Breitkreuz, C. 2019. Coulomb failure of Earth's brittle crust controls growth, emplacement and shapes of igneous sills, saucer-shaped sills and laccoliths. *Earth and Planetary Science Letters*, **510**, 161-172, https://doi.org/https://doi.org/10.1016/j.epsl.2019.01.011.

Senger, K., Betlem, P. *et al.* 2021. Using digital outcrops to make the high Arctic more accessible through the Svalbox database. *Journal of Geoscience Education*, **69**, 123-137, https://doi.org/10.1080/10899995.2020.1813865.

Sleveland, A.R.N., Midtkandal, I., Galland, O. and Leanza, H.A. 2020. Sedimentary Architecture of Storm-Influenced Tidal Flat Deposits of the Upper Mulichinco Formation, Neuquén Basin, Argentina. *Frontiers in Earth Science*, **8**.

Visage, S., Souloumiac, P., Cubas, N., Maillot, B., Antoine, S., Delorme, A. and Klinger, Y. 2023. Evolution of the off-fault deformation of strike-slip faults in a sand-box experiment. *Tectonophysics*, **847**, 229704, https://doi.org/https://doi.org/10.1016/j.tecto.2023.229704.

Figures

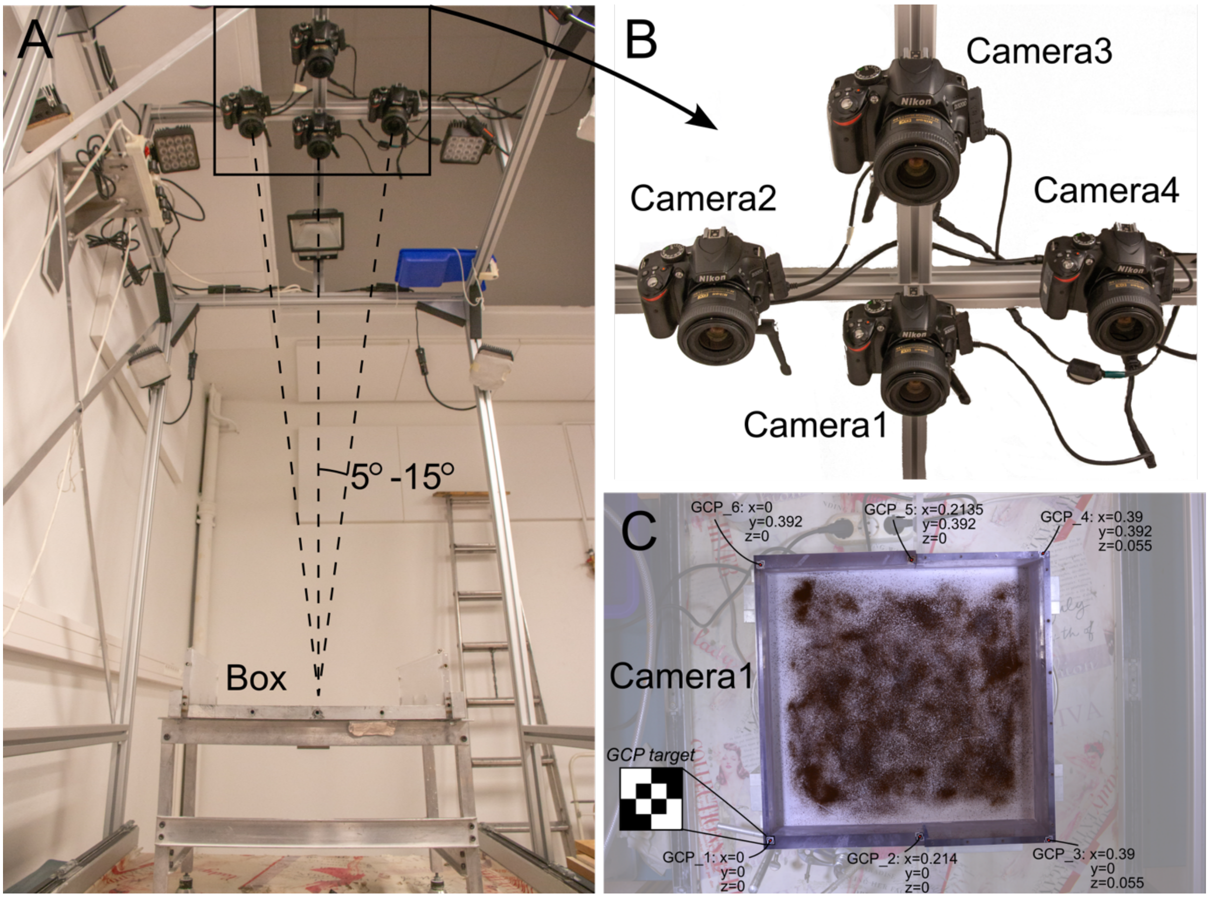

Figure 1. A. Photograph of example laboratory setup showing camera positions with respect to sandbox. Angle between cameras axes should range between 5° and 15°. B. Close-up photograph of cameras. Here, Camera1 is central one, pointing vertically downwards. C. Example of photograph taken by central Camera1 of initial condition of a magma emplacement model. Note that the image outside the box was made partly transparent. The non-uniform texture at the model surface was created by sieving instant coffee and olivine sand on top of white silica flour. Six Ground Control Points (GCPs) with their (x,y,z) coordinates are located around model box. Note that GCPs 3 and 4 are placed on a higher wall of the box than the others GCP, as reflected on their different z coordinates. The definitions of these GCPs for georeferencing in MicMac are presented in **Error! Reference source not found.** and in section “Georeferencing the models”.

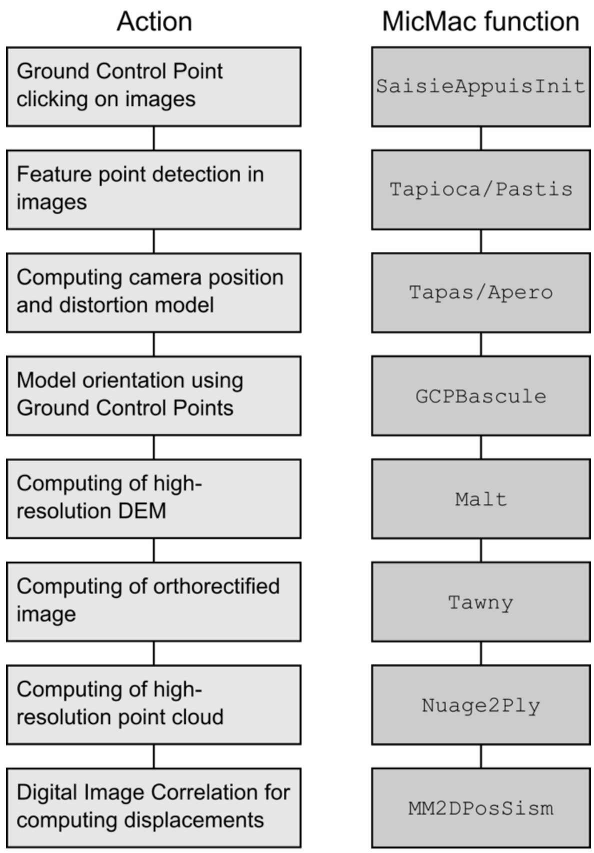

Figure 2. Workflow chart of successive steps of MicMac workflow described in this study. Left column: actions. Right column: corresponding MicMac function. See detailed description in Table 4.

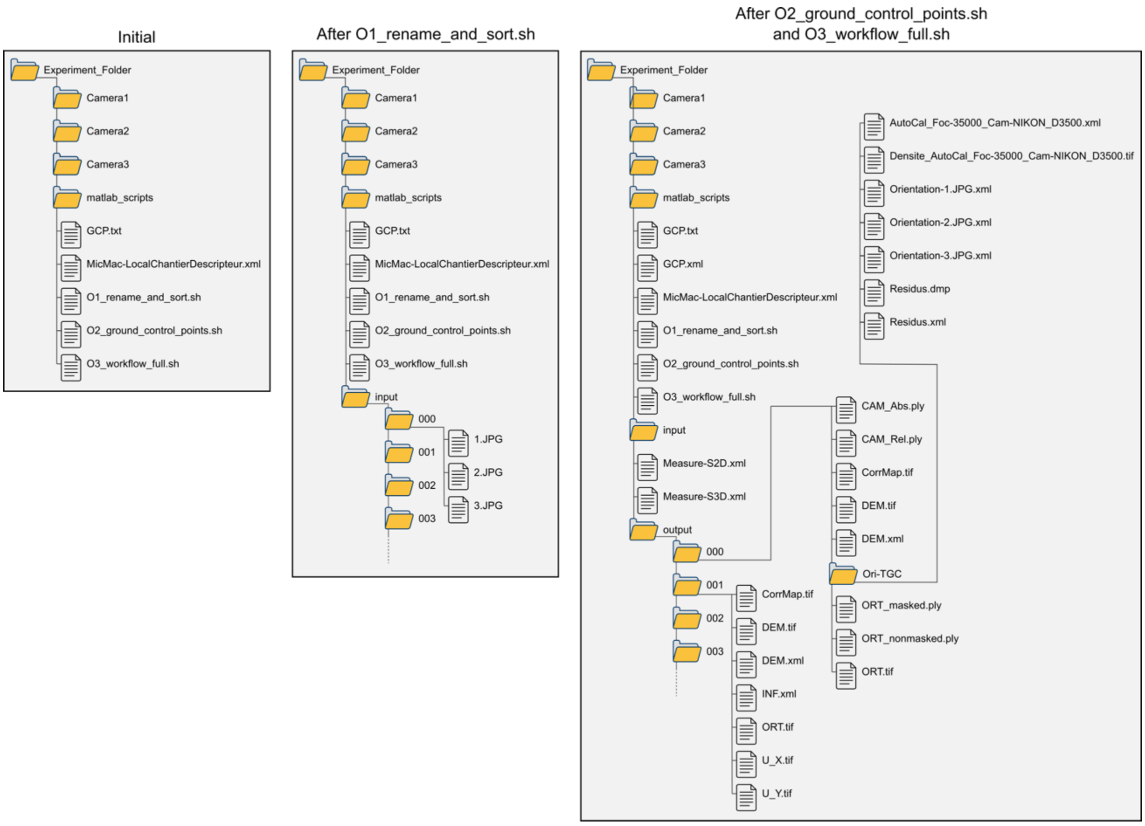

Figure 3. Example of folder chart structure of experiment folder for a laboratory setup with three cameras. Left: initial folder structure. Centre: after running `O1_rename_and_sort.sh`. Note the folders *000*, *001*, etc., in folder *input* correspond to a case with 3 cameras. Right: after running `O2_ground_control_points.sh` and `O3_workflow_full.sh`.

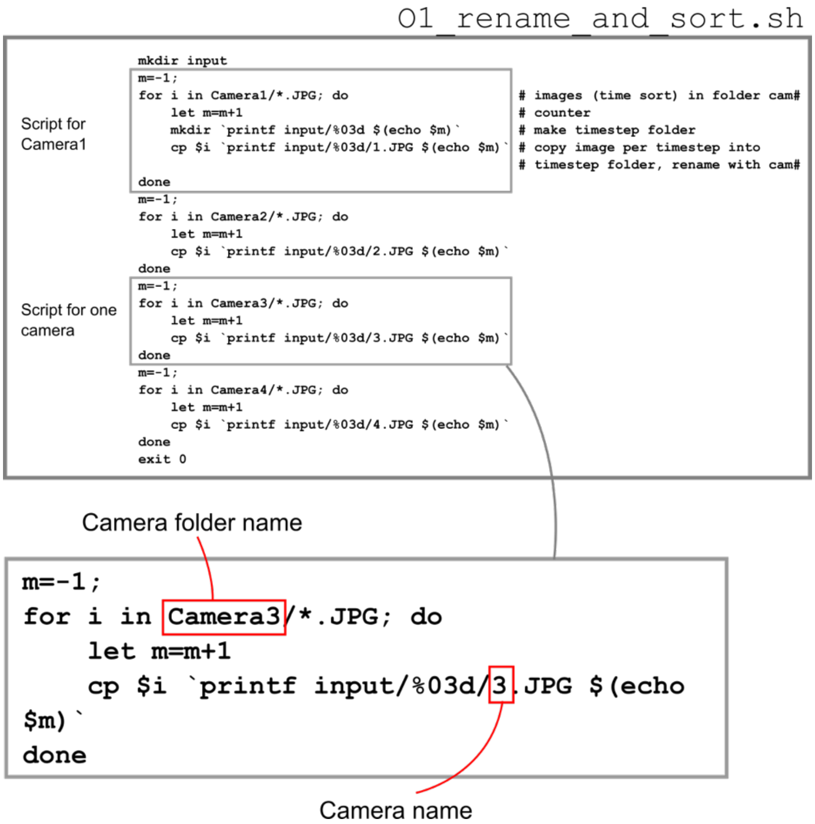

Figure 4. Example of structure of shell script `01_rename_and_sort.sh` for a setup with three cameras.

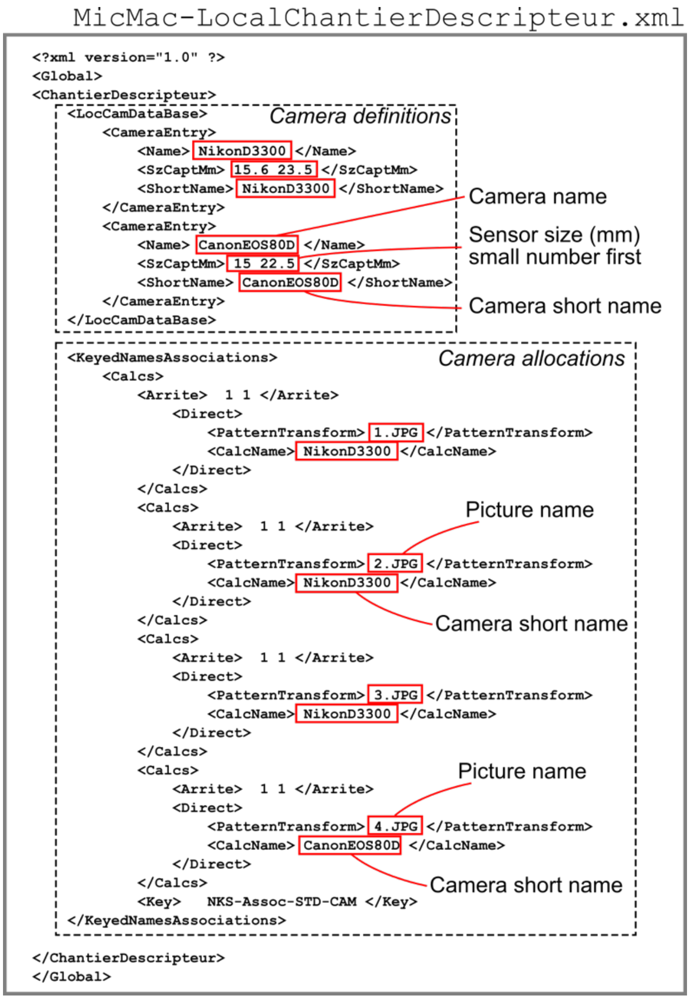

Figure 5. Characteristic example of the structure of file `MicMac-LocalChantierDescripteur.xml` to define the cameras used in the photogrammetry system, their sensor size and which picture they shot.

`03_workflow_full.sh`

```
#!/bin/bash

#Enter the path to folder micmac/bin
export PATH=/Applications/micmac/bin:$PATH

# Manual input and user preferences
BOX='[0.1,0.1,0.3,0.3]' # set cropbox size [x_min,y_min,x_max,y_max]
INIT="0"
NrofIm="63" # Set number of timesteps
Uncertainty="5" # Set size of exploration window for Digital Correlation
SizeCorrWind="4" # Set size of correlation window for Digital Correlation
...
```

Figure 6. First lines of shell `script 03_workflow_full.sh` showing the variables to choose by the modeller. Note that the path to `micmac/bin` needs to be changed by the modeller, to ensure that the script calls the MicMac functions.

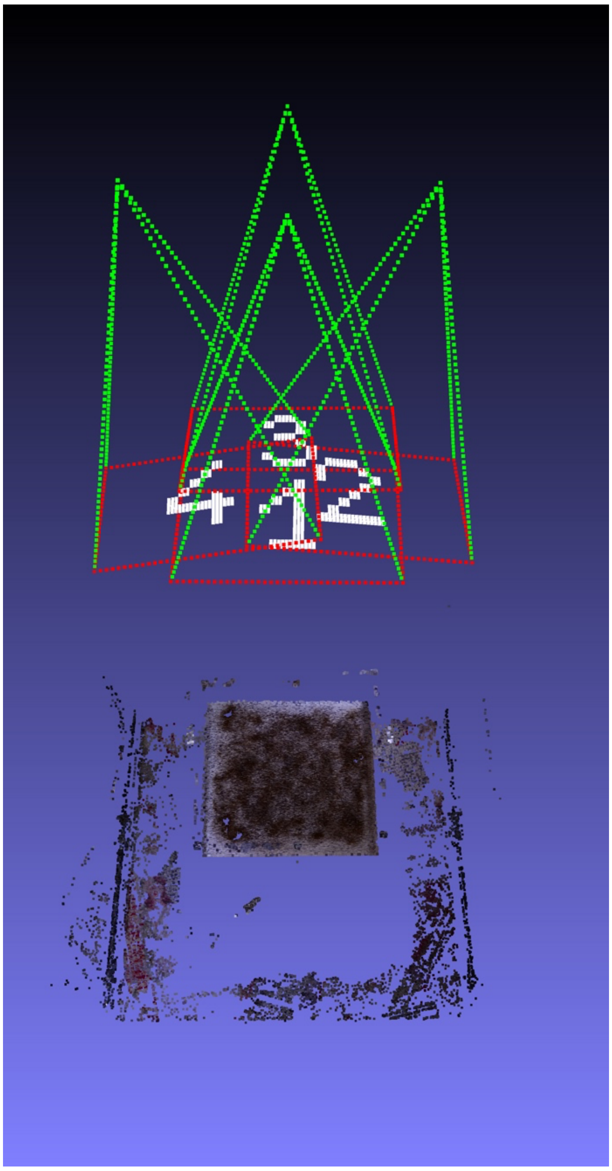

Figure 7. Screenshot of a characteristic point cloud of tie points (file CAM_Abs.ply) computed from experiment described in Figure 9. Software used to display the point cloud is open-source Meshlab. The red and green features with white numbers correspond to camera position and number. Photograph of Figure 1c (shot from Camera1) has been used to produce this point cloud together with images from three other cameras: one can recognize the square model surface with texture, and the surrounding background.

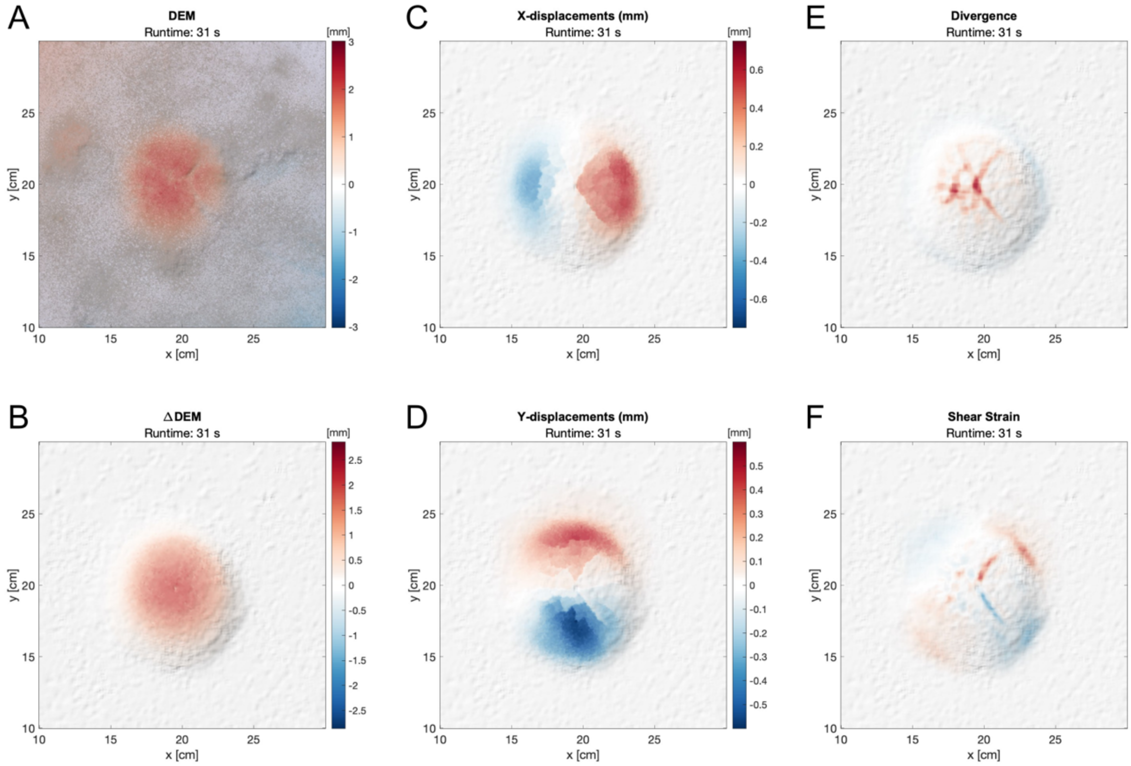

Figure 8. Characteristic plot examples of surface data of magma intrusion experiment. A. DEM with background image and shaded relief calculated from DEM. B. U_DEM without background image and with shaded relief calculated from U_DEM data. C-F. U_X, U_Y, divergence and shear strain with background image and shaded relief.

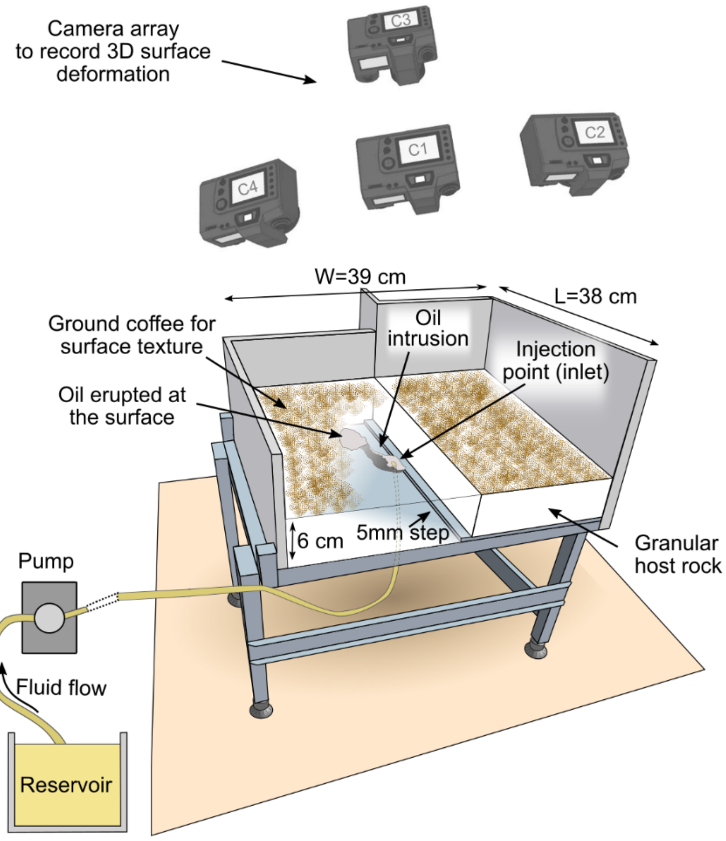

Figure 9. Experimental setup to model dyke-induced surface deformation.

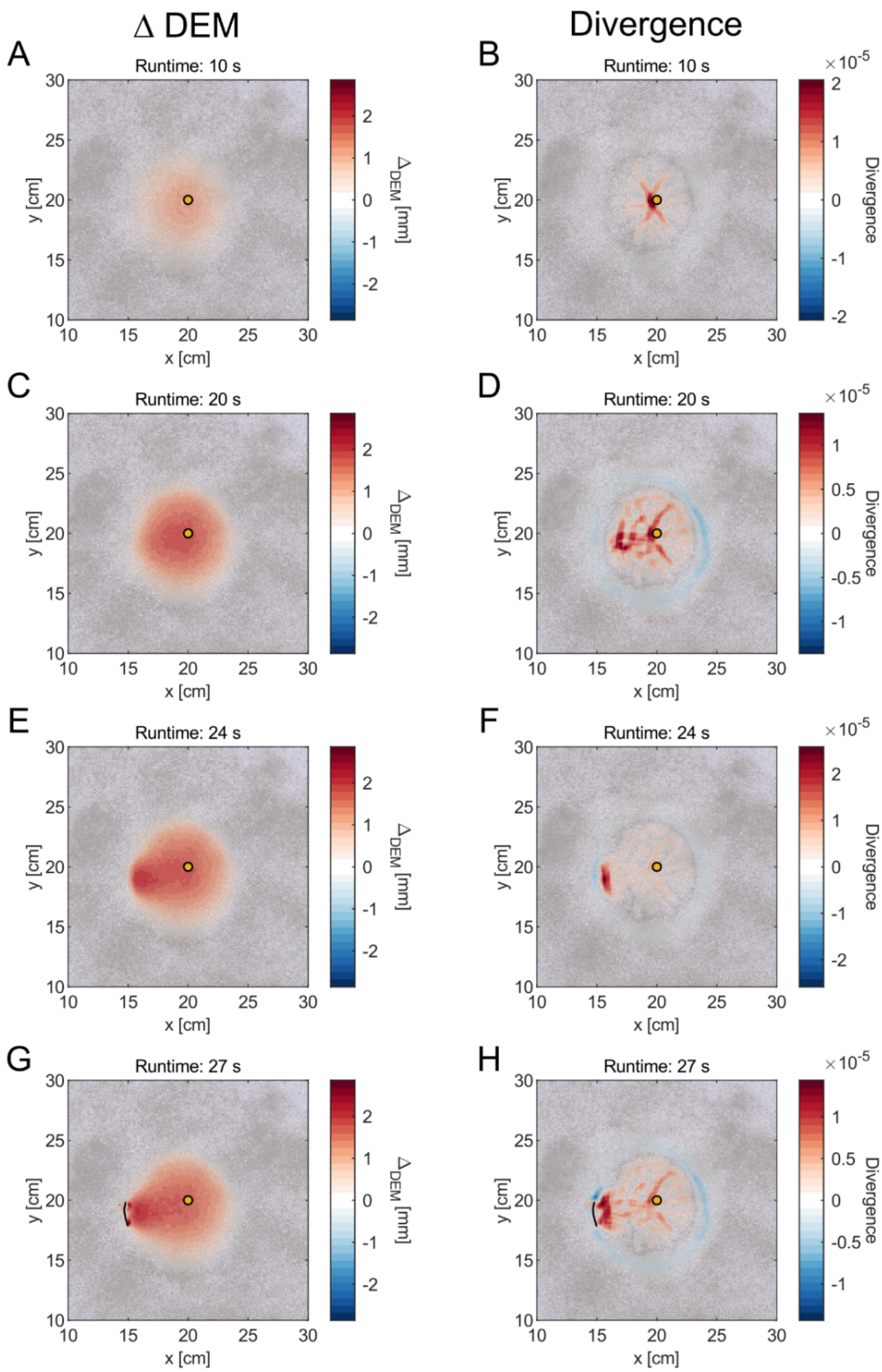

Figure 10. Cumulative vertical surface deformation (A, C, E and G) and horizontal divergence (B, D, F and H) at four different time steps with corresponding background images. Note that the color scales of the divergence plots vary in each panel. The yellow circle marks the surface projection of the injection inlet, where the oil enters the base of the box. The black line in panels G and H marks where the oil breached the surface, i.e., where the "eruption" occurred.

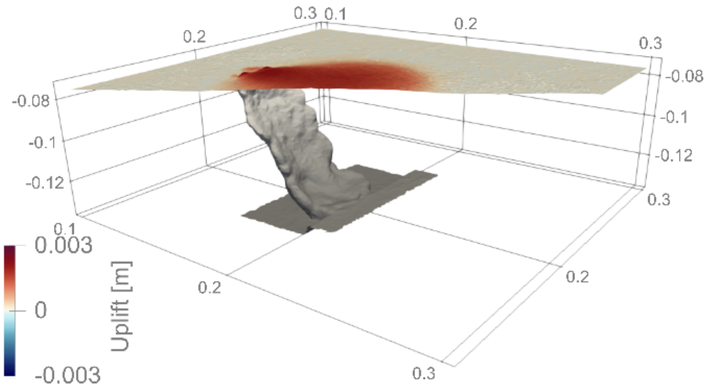

Figure 11. Virtual 3D model of the final oil intrusion and the associated final vertical surface deformation. From injection to the surface the intrusion crossed a depth range of 6 cm.

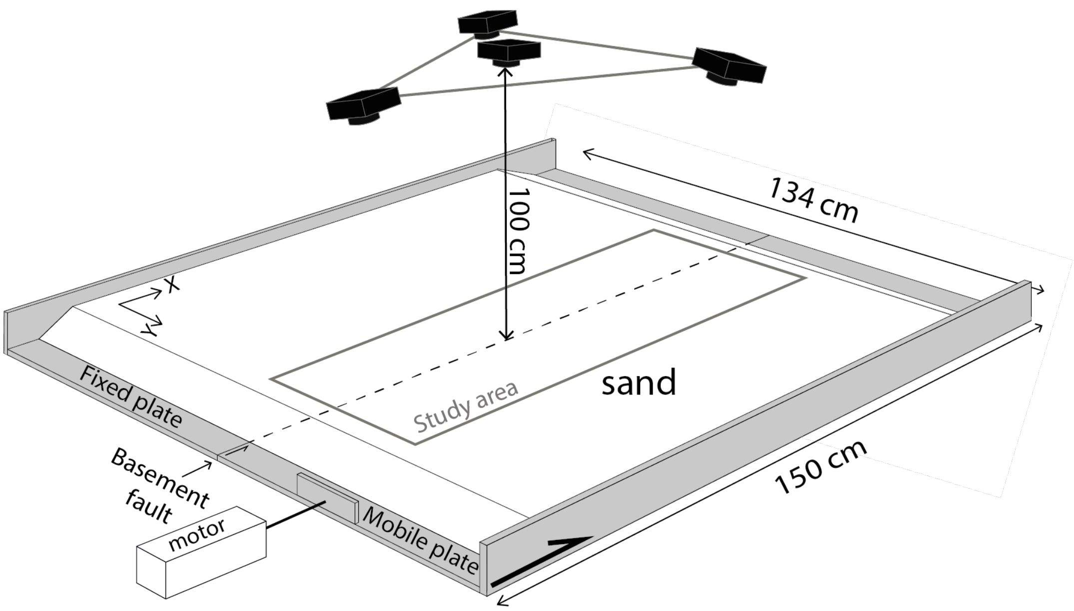

Figure 12. Experimental sandbox set-up of the Lab GEC (CYU) for strike-slip fault with cameras above the box. The grey rectangle represents the study area for the surface deformation analysis. Modified from Visage *et al.* (2023).

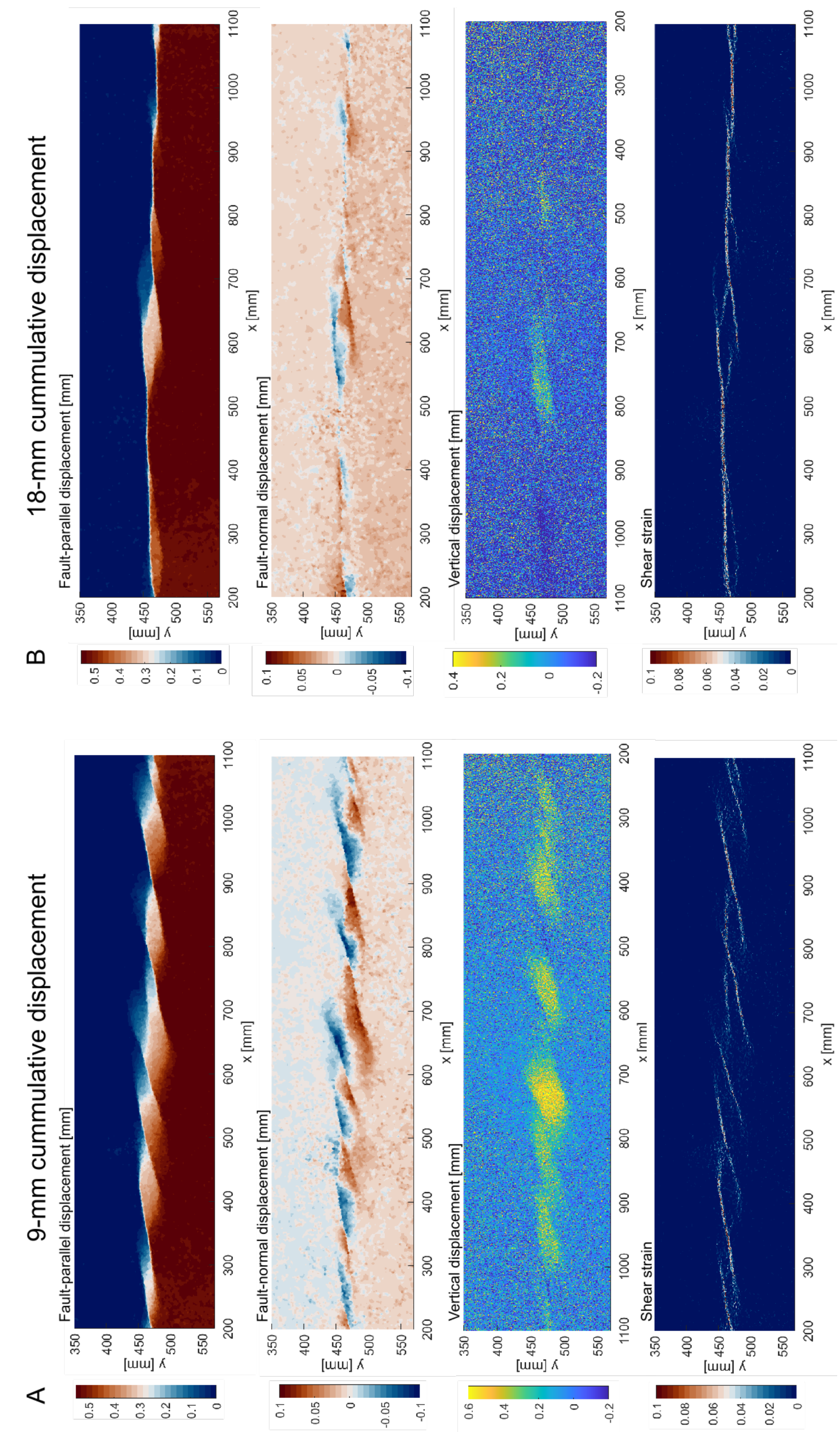

Figure 13. A. Optical image monitoring results at 9 mm of cumulative displacement. B. Optical image monitoring results at 18 mm of cumulative displacement. Both A and B. Top row: fault-parallel

displacement; Second row: fault-normal displacement; Third row: vertical displacement; Bottom row: shear deformation.

Tables

Table 1. List of steps necessary for the preparation of the model surface and of the monitoring system.

Task	Purpose and relevance	Implementation
Texture at model surface	Structure-from-Motion is based on analysing features in the processed images, which therefore need to contain features and texture (see Appendix D: https://archive.sigma2.no/pages/public/datasetDetail.jsf?id=10.11582/2024.00066, folder 4_Appendix).	Common materials used in sandbox models, such as white sand and white silica powders, are rather homogeneous in colour and display very little texture. It is necessary to add texture to the surface of the models. We commonly sieve instant coffee (note that coffee beans may stain, do not use them if the model is going to be moistened for later sectioning) or olivine sand. The results of the photogrammetry will depend on the quality of the texture (see Appendix D; https://archive.sigma2.no/pages/public/datasetDetail.jsf?id=10.11582/2024.00066, folder 4_Appendix). That there is no need to make a homogeneous texture
Ground Control Points (GCPs)	GCPs are essential to make the data properly oriented and scaled	Place targets around the model and measure their precise (X,Y,Z) coordinates in meters to use as inputs for the georeferencing (Figure 1c). A minimum of 4 GCPs, preferably located slightly outside the model surface around the corners of the model, is necessary for a robust georeferencing
Monitoring system	Three or more synchronized cameras of any type are necessary. It is preferable that the camera set is of the same model, though different camera models would theoretically work.	We have used standard DSLR cameras, but GoPro (or equivalent) cameras can be used, as well as fast cameras, as long as they are synchronised. If the same camera model is used, we highly recommend using lenses with fixed focal length on all cameras. Given the various available camera types and triggering systems, these will be laboratory-dependent and so we will not develop this aspect further
Camera positions	Structure-from-Motion implies that a 3D structure of an object can be reconstructed from images taken from distinct view points. Cameras should thus be placed to fullfil position criteria.	(1) The distance should be large enough to ensure that the GCPs are visible from all cameras (Figure 1c). (2) The positioning of the cameras should be the following: one camera should be placed vertically above the model; this will be called *Camera1* (Figure 1b). Others can be placed around *Camera1* with converging views toward the centre of the models. The distance between the cameras is such that the angle between the camera axes should be between 5° and 15° (Figure 1a)
Framing rate	It is important to set the framing rate properly to compute horizontal displacements. MicMac function for computing horizontal displacements can detect displacements smaller than a maximum value.	The maximum displacement value detected by MM2DPosSism is set by option Inc, described in section "Structure-from-Motion". If displacements between two acquisitions are larger than this maximum value, displacements will not be calculated properly. The modeller needs to adjust the framing rate such that the displacements in pixels between two acquisitions are smaller than the maximum value.

Table 2. Description of successive steps of camera calibration.

Step 1	Place a target near the middle of the model.
Step 2	Place Camera2 (or any camera different than Camera1) at the location of Camera1. Adjust the stand such that the target is at the central focus point of the camera. On Autofocus mode, make focus on the target. Once focus is done, switch the lens to Manual Focus mode. Move the calibrated camera to its position during the run of the model, without touching the lens in order to avoid disturbing the focus. Operate similarly with all other cameras except Camera1.
Step 3	For Camera1, place the camera at its position. Adjust the stand such that the target is at the central focus point of the camera. On Autofocus mode, make focus on the target. Once focus is done, switch the lens to Manual Focus mode. Do not move the camera.
Step 4	The cameras are calibrated. Once this is done, format all memory cards to make sure there is no image in the card at the beginning of the experiment.

Table 3. Instructions for installing MicMac on different OS.

Linux	Installing MicMac on a modern Linux distribution is very straightforward. Appendix A (https://archive.sigma2.no/pages/public/datasetDetail.jsf?id=10.11582/2024.00066, folder 4_Appendix) lists the sequence of command lines needed to get it running on Ubuntu 24.04, which should require minimal edits to be ported to other distributions.
Windows	As explained above, we provide only Bash scripts that call MicMac functions, so that these scripts cannot be used directly on Windows command shell. Instead, we invite the modeller to install Windows Subsystem for Linux (WSL) as a form of virtual machine running Ubuntu on Windows. Instructions to install WSL can be found on the following webpage: https://learn.microsoft.com/en-us/windows/wsl/install, and select the latest Ubuntu version to install. Once WSL is installed, the instructions for Linux (see above and Appendix A: https://archive.sigma2.no/pages/public/datasetDetail.jsf?id=10.11582/2024.00066, folder 4_Appendix) can be followed to install MicMac in WSL.
MacOS	Installing MicMac on MacOS is done through a series of command lines to run in a Terminal window. The instructions can be followed in the following YouTube tutorial (https://youtu.be/eRjqWpHShIs). Appendix B (https://archive.sigma2.no/pages/public/datasetDetail.jsf?id=10.11582/2024.00066, folder 4_Appendix) also lists the sequence of commands to run to install MicMac on MacOS.

Table 4. List of MicMac functions used in the presented in this study.

Functions	Relevance and implementation
Tapioca/Pastis	Calculates Tie points in image set. Tie points are SIFT (Scale-Invariant Feature Transform) feature points (Lowe 2004) that are common to, at least, two of the processed images. in brightness intensity: continuous gradients or small amplitude peaks would not yield tie points. Therefore, the combined camera resolution/size of features on the model surface should lead to sharp, prominent features in the processed images.
Tapas/Apero	Tie points are used in a Structure-from-Motion (SfM) bundle adjustment to automatically compute both the external orientations (camera positions and viewing angle) and the internal orientation (camera calibration)
GCPBascule	Scales and orient models using Ground control points (GCPs). We use targets taped in top of the walls of the box, preferably near the corners, as GCPs (Figure 1C). In general, GCPs do not need to correspond with tie points. A minimum of 3 GCPs visible on at least two images are necessary for this (geo)referencing.
Malt	Computes high-resolution reconstruction through image correlation, yielding a depth map, i.e. a DEM. Points are computed on a regular grid of the interest area, regardless of the positions of the tie points calculated with Tapioca. Spatial resolution of the DEM will be close to half of images' ground sampling distance (GSD). Image correlation requires that model surface does not display homogeneous pixel patches bigger than the correlation window, which defines the template for which correlation is computed for the templates corresponding to each pixel of the search window. Prominent features used for computing tie points are relevant, as well as smoother features such as gradients.
Malt/Tawny	Computes orthorectified [Malt] and mosaicked [Tawny] image based on camera positions, camera calibration and the DEM computed in the previous step. Orthorectified image is a geometrically corrected ("orthorectified") photograph such that the scale is uniform: the photo has the same lack of distortion as a map. Unlike a normal photograph, an orthorectified image can be used to measure true horizontal distances, because it is an accurate representation of the photographed surface, having been adjusted for topographic relief, lens distortion, and camera tilt.
Nuage2Ply	Computes high-density point cloud by integrating DEM and orthorectified image.
MM2DPosSism	Implement high-quality digital image correlation (DIC) between two images, to compute sub-pixel, high-resolution in-plane displacement maps at the surface of deforming objects (Rosu *et al.* 2015). Every pixel of the image is systematically tracked, regardless of the prominence of the local pattern of pixels; the correlation would fail in the absence of feature. Patterns seen in the images are not tie points calculated from Tapioca. DIC applied to ortho-rectified images to compute true displacements.

Table 5. List of variable parameters in script `03_workflow_full.sh`.

Parameter	**Meaning**
BOX='[x_min,y_min,x_max,y_max]'	Sets boundaries of a rectangular mask in coordinate system defined by georeferencing. Variables x_min and y_min define coordinates of lower left corner of rectangular mask, whereas x_max and y_max define its upper right corner.
INIT="0"	Number of folder of initial time step of model. Default number 0 means folder *000*. Note that number does not display zeros before 0, but script will recognise that it will be folder *000*. If monitoring of experiment starts after 2 camera shootings, enter INIT="2" and processing will start at folder *002*.
NrofIm="63"	Number corresponds to name of last time step folder in *input* folder. Note that number does not display zero before 63, but script will recognise that it will be folder *063*.
Uncertainty="4"	Size of exploration window for digital image correlations calculations using MM2DPosSism function. This parameter is linked to maximum displacement U_{max} in pixel that can be computed with MM2DPosSism: U_{max} = Uncertainty*1.41. For instance, if Uncertainty="4", maximum displacement that can be detected is ~5.64 pixels. Modeller should thus adjust (1) framing rate of the monitoring, (2) resolution of images and (3) deformation rates in case of tectonic experiments such that displacements in pixels between two acquisitions is always below maximum detectable value. Note that duration of digital image correlation is exponentially correlated to value of Uncertainty, thus we recommend keeping a relatively low value (<6) to avoid slowing down calculations.
SizeCorrWind="3"	Size of correlation window in pixels for digital image correlation calculations using MM2DPosSism function. Number *i* corresponds to correlation window of size $2 \times i + 1$ pixels (Rosu *et al.* 2015). Size of correlation window links with characteristic size of features on the model surface. If patterns on model surface is 15 pixels, correlation window of 5 pixels will be too small for capturing displacements of 15-pixel features, and resulting displacement maps will be noisy.

Table 6. List of output files produced from script `03_workflow_full.sh`.

Folder 000	
CAM_Abs.ply	Displays georeferenced tie points and camera positions computed from Tapas (Figure 7). Opening this file allows assessing if the result of the SfM calculation was correct. It also allows assessing whether there is enough feature on the model surface. Note that .ply files can be opened with open-source software CloudCompare or Meshlab.
CAM_Rel.ply	Displays tie points and the camera positions computed from Tapas before georeferencing.
CorrMap.tif	Displays correlation map of the calculated DEM (DEM.tif). The brighter the pixels, the better the correlation. Correlation map allows identifying which parts of model surface provide the best correlation, which can be used for improving surface preparation (see section "Improving data quality from existing tests").
DEM.tif	Contains Digital Elevation Model data. Note, however, that data needs to be converted with parameters stored in *DEM.xml*.
DEM.xml	Contains information for scaling DEM. Parameters include: (1) NombrePixels, provides pixel numbers along horizontal (first number) and vertical (second number) axes; (2) OriginePlani, sets x and y coordinates of upper left pixel of the DEM; (3) ResolutionPlani, provides horizontal (first number) and vertical (second number) sizes of pixels (in meters) of DEM; (4) OrigineAlti, sets reference elevation in DEM; (5) ResolutionAlti, provides resolution of elevation data. Matlab codes calculate true topographic data using formula DEM × ResolutionAlti + OrigineAlti. Note that parameters in *DEM.xml* are automatically read by Matlab scripts described in section "Loading and plotting the data".
Ori-TGC	Folder that contains calculated results of distortion model (*AutoCal_Foc-35000_Cam-NIKON_D3200.xml*), camera positions (*Orientation-i.JPG.xml*) and quality of SfM calculation (*Residus.xml*). In *Residus.xml* file, values of Residual for four cameras provide indications of quality of SfM calculations: Residual values between 0.3 and 0.5 is very good, lower values are excellent. In our laboratory, we achieve SfM calculations with Residual<0.2.
ORT_masked.ply, ORT_nonmasked.ply	High-resolution point clouds of the model surface within the masking area.
ORT.tif	Orthorectified image of masking area computed by MicMac. Orthorectified image is used by digital image correlation function MM2DPosSism to compute displacements U_x and U_y.
Folder 001 and subsequent	
CorrMap.tif, *DEM.tif*, *DEM.xml*, and *ORT.tif*, which have the same meaning and definitions that in folder *000*.	
U_X.tif and *U_Y.tif*	Maps of horizontal and vertical displacements, respectively, in pixels, if user decides to compute them.
INF.xml	File containing information of *U_X.tif* and *U_Y.tif* maps. Most important is NombrePixel, which provides number of pixels in horizontal (first number) and vertical (second number) axes. Note that there is systematically one pixel less than in DEM maps.

Table 7. List of Matlab scripts and description of their function.

Code name	Function
O0_Master_code.m	Code to run by the user. None of the other codes need to be run by the user.
O1_input_parameters.m	User can give the relevant parameters of the maps. To modify the parameters, just open O1_input_parameters.m and modify manually the values of the listed parameters.
O2_DEM_load_scale.m	Loads all DEMs and calculates all U_DEMs, and calculates and stores the highest and lowest values to set the colour in the maps.
O3_DEM_plot.m	Plots DEM and U_DEM maps. The user is offered the option to plot the data on transparency over (1) the orthorectified image and/or (2) a shaded relief map to provide relief to the maps.
O4_Displacement_load_scale.m	Loads all U_X, U_Y and calculates divergence and shear strain maps, and calculates and stores the highest and lowest values to set the colour in the maps.
O5_displacement_strain_divergence_plot.m	Plots U_X, U_Y and calculates divergence and shear strain maps. The user is offered the option to plot the data on transparency over (1) the orthorectified image and/or (2) a shaded relief map to provide relief to the maps.
O6_MovieAndGifAnimator.m	Produces animation files of the maps in .mp4 format.

Table 8. List of input variable parameters in Matlab script `O1_input_parameters.m`. These parameters allow the modeller to plot data maps with versatile layout.

Parameter	**Meaning**
xMin, xMax, yMin, yMax	Define bounding coordinates of topographic and displacement maps. They correspond to bounding values of mask defined in script “O3_workflow_full.sh” at line 7 to set bounding box of working mask.
tick_inc	Sets increment in meters between ticks along axes of maps.
unit_ticks, unit_colorbar_DEM, unit_colorbar_U_DEM, unit_colorbar_disp	Set units of data and of axes of maps. Variable *unit_ticks* sets unit of axes of maps, variable *unit_colorbar_DEM* sets unit of DEM data and colourbar, variable *unit_colorbar_U_DEM* sets unit of differential DEM data and colourbar, and variable *unit_colorbar_disp* sets unit of displacement data and colourbar. Note that data are always in meters, but their values in maps are corrected according to chosen units.
inc_color	Sets resolution of colour scale of plots. Colour scale is set to be blue for negative values and red for positive values, and white value zero. If *inc_color* = 1, colour scale is separated in 32 colour increments from deep blue to deep red. If *inc_color* > 1, number of colour increments of colour scale will be 32×*inc_color*, i.e. higher colour resolution.
x0, y0, width_fig	Define size and position of figure in screen. Location of lower left corner of figure is given by *x*0 and *y*0, while width of figure is given by *width_fig*, unit being in pixels.
time_unit, time_inter,	Define specific aspects of time reference and time resolution of data to be displayed in maps. Parameter *time_unit* sets time unit in either seconds (*‘s’*), minutes (*‘min’*) or hours (*‘hour’*). This parameter will be chosen adequately with time resolution of acquisition during experiments. Parameter *time_inter* sets time interval between two acquisitions in time unit defined by *time_unit*. If time interval between acquisition is 2 seconds, *time_unit=’s’* and *time_inter*=2, whereas if time interval is 3 minutes, *time_unit=’min’* and *time_inter*=3.
time_start_exp, t0	Allows user to exclude some of first folders of analysis. For example, if experimental setup requires two steps of acquisition before start of experiment, *time_start_exp*=2. However, in most cases *time_start_exp*=0. This number is same as INIT parameter in script O3_workflow_full.sh (Figure 6; see section Structure-from-Motion). Finally, parameter *t*0 defines time delay of the effective start of an experiment. An example is given by magma injection experiments of Schmiedel *et al.* (2019), injection pipes are not entirely filled with magma analogue. Thus, in these experiments beginning of experimentation (and of acquisition) starts with filling of the injection systems, then analogue magma injection starts after delay *t*0 after start of experiment. With this parameter, user can plot only data after effective start of model.
reference_DEM	Allows user to choose reference elevation of DEM maps. If *reference_DEM* = 1, reference of the DEM is elevation of the GCPs. Conversely, if *reference_DEM* = 0, DEM will be translated such that average elevation of the corners of DEM are set to 0.
thresholdDEM, thresholdUDEM	Allow user to either remove outliers resulting from low quality photogrammetric results or remove some unwanted parts in DEM and U_DEM maps. For example, in tectonic experiments, a movable piston that triggers compression will appear in topographic maps, and vertical walls will degrade maps and colour scale. If for example, maximum altitude of sandbox model surface is h_s and height of a movable wall is h_w and h_s > h_s, chosing a value of *thresholdDEM* between h_w and h_s allows removing the pixels in map that correspond to moving piston.
thresholdU, smooth_displ, smooth_div	Define properties for optimal display of U_x and U_y maps. Parameter *thresholdU* is a threshold that filters artifacts that lead to unrealistic, too large horizontal displacements. Parameter *smooth_displ* allows smoothing U_x and U_y data using moving average. It implements smooth2a.m function (Reeves 2023). Value of *smooth_displ* corresponds to size in pixels of moving averaging window, and so value of *smooth_displ* should always be 1 or larger. Large values of *smooth_displ* will lead to large smoothing of data noise but also potentially remove important data such as sharp displacement gradients associated with fractures at model surfaces. Unless data is not very noisy, we advise to use *smooth_displ*=1. Parameter *smooth_div* allows smoothing divergence and shear strain maps, calculated from gradients of U_x and U_y, using moving average. Value of *smooth_div* corresponds to size in pixels of the moving averaging window, and so value of *smooth_div* should always be 1 or larger. We advise to use *smooth_div* between 5 and 15, depending on spatial resolution and noise level of data.
DEM_background_image, DEM_hillshade	Indicate whether modeler wants to plot (1) orthorectified image of model surface and/or (2) shaded relief map, respectively, as background of DEM maps. Programs use hillshade.m function (Hebeler 2023).
U_DEM_background_image, U_DEM_hillshade, U_DEM_hillshade_U_DEM	Indicate whether modeler wants to plot (1) orthorectified image of model surface and/or (2) a shaded relief map, respectively, as background of U_DEM maps. If *U_DEM_hillshade* = ‘yes’, modeller can choose whether shared relief is calculated from DEM or U_DEM data using parameter *U_DEM_hillshade_U_DEM*.
disp_background_image, disp_hillshade, disp_hillshade_U_DEM	Indicate whether modeler wants to plot (1) orthorectified image of model surface and/or (2) a shaded relief map of DEM, and/or (3) or a shaded relief map of U_DEM, respectively, as background of the U_X, U_Y, divergence and shear strain maps.
disp_symmetry	Allows modeller to impose symmetrical colour scale for displacement maps. For example, in characteristic strike-slip fault models (see for example section "Strike-slip faulting experiment"), boundary conditions are commonly non-symmetrical, with one moving part of box while other remains static. Consequently, static part of model will display zero displacements, while moving part of model will display large displacement. If *disp_symmetry* = ‘yes’, code will correct maps such that static and the mobile parts of the models display opposite displacements of similar absolute values (see example in Figure 13).
smooth_hillshade_DEM, smooth_hillshade_U_DEM	Set smoothing options of shaded relief patterns in plotted maps.